Title

THE EFFECT OF THE PRECIPITATE SIZE DISTRIBUTION ON THE AGING CURVE OF ORDER HARDENING ALLOYS

Author

Morris, J.W.

Publication Date

1987-02-01

LBL-23047
Preprint

Lawrence Berkeley Laboratory
UNIVERSITY OF CALIFORNIA

Materials & Chemical Sciences Division

Center for Advanced Materials

Submitted to Acta Metallurgica

THE EFFECT OF THE PRECIPITATE SIZE DISTRIBUTION ON THE AGING CURVE OF ORDER HARDENING ALLOYS

J. Glazer and J.W. Morris, Jr.

February 1987

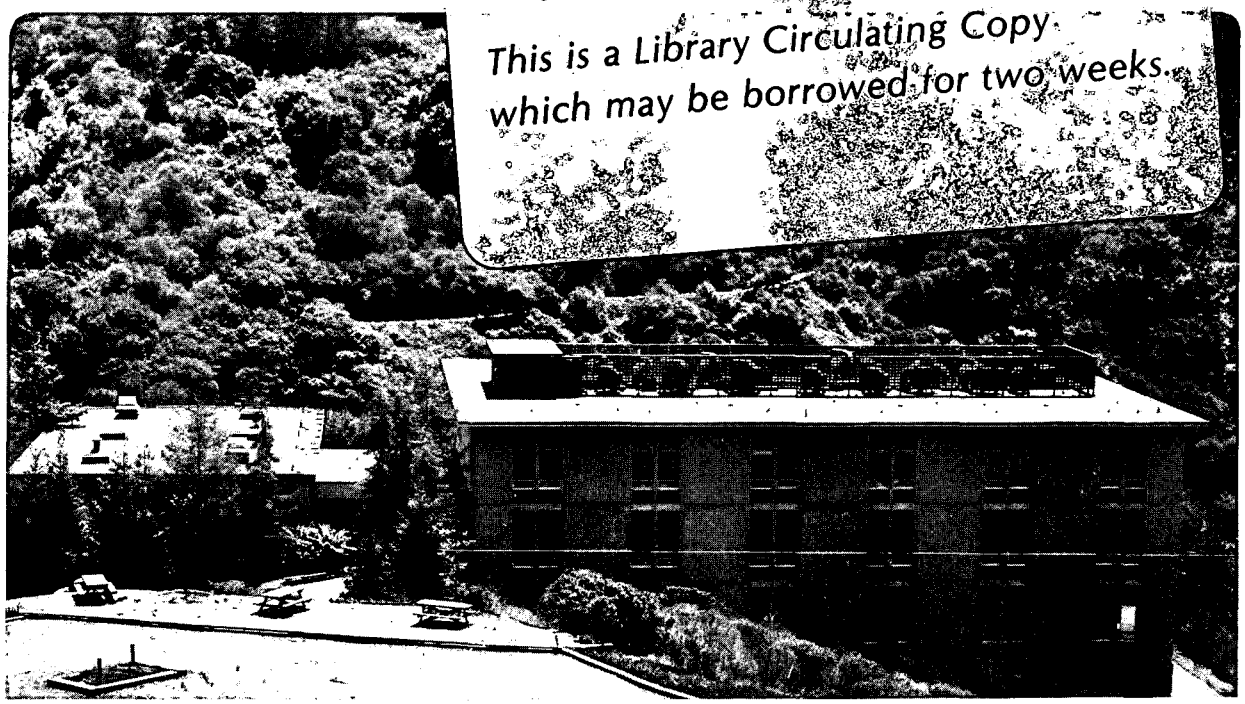

Prepared for the U.S. Department of Energy under Contract DE-AC03-76SF00098

DISCLAIMER

The Effect of the Precipitate Size Distribution on the Aging Curve of Order Hardening Alloys

J. Glazer and J. W. Morris, Jr.

Department of Materials Science and Mineral Engineering,
University of California, and Center for Advanced Materials,
Lawrence Berkeley Laboratory, Berkeley, California 94720

Abstract

The effect of the shape of the precipitate size distribution on the age-hardening behavior of alloys strengthened by ordered precipitates is investigated using a modified version of the Hanson and Morris strong line model for the critical resolved shear stress. This model accounts for the influence of dislocation self-interactions on the effective strength of obstacles to dislocation glide. The model predicts that the largest precipitates are responsible for the peak in strength, but that the value of the peak strength is determined principally by the average precipitate radius at peak strength. The peak strength for a given volume fraction is maximized if all of the precipitates are the same size. These qualitative results are used to interpret existing data on the effect of the precipitate size distribution. The contributions of obstacles of differing strengths are included through a quadratic sum rule. Binary aluminum-lithium alloys are used as a model system with which to examine the quantitative accuracy of the model.

1. Introduction

The age-hardening behavior of a material strengthened by a precipitates of varying size has been modeled by Melander and Persson [1-3]. The effect of the shape of the precipitate size distribution on the critical resolved shear stress at a fixed average precipitate size has also been considered [4]. However, the consequences of the precipitate size distribution shape for aging behavior have not been investigated in the context of a model suitable for treating strong obstacles to dislocation glide. Since the precipitate size distribution about an average diameter <d> can be varied by heat treatment [4,5], the effect of the distribution on aging behavior is of practical importance. This paper will examine the influence of the shape of the precipitate size distribution on the aging response of materials hardened by strong shearable precipitates. The role of the largest precipitates in the distribution on behavior near peak strength is specifically discussed.

The critical resolved shear stress is modeled in this investigation using the extension of the Hanson and Morris "strong line" model [6] developed by Glazer and Morris [7] for materials hardened by a random array of strong ordered precipitates. The problem is approached by representing the precipitate size distribution as a distribution of obstacles to dislocation glide of varying strengths. Any quantitative strengthening theory must be able to account for the effects of such an obstacle strength distribution since there will always be a distribution of obstacle strengths in any real material (even monodisperse spherical

particles are cut at various cross sections [8]). The effect of the distribution of obstacle strengths, not dealt with by Glazer and Morris [7], is included through the quadratic sum rule derived by Hanson and Morris [6]. Binary aluminum-lithium alloys are used as a model system with which to check the quantitative accuracy of the model.

2. The Critical Resolved Shear Stress of a Random Array of Distinct Obstacles

The development of the critical resolved shear stress model used in this work is described in detail by Hanson and Morris [6], Glazer and Morris [7], and Glazer [9] and is summarized only briefly below. Other relevant work in this area is summarized in a recent review by Ardell [8]. The solution considers the critical resolved shear stress of a dislocation gliding athermally in a random array of point obstacles. The dislocation, modeled as a flexible and extensible string of constant line tension, bows out in a circular arc between the obstacles. Poisson's ratio is taken to be zero. The properties of the point obstacles are adjusted so that the interaction between the mathematical point and dislocation is identical to the interaction between the physical obstacle and dislocation. The strength of the obstacle corresponds to the peak in the force-distance curve for the physical dislocation-precipitate interaction, and is given by $\beta = F/2T = \cos(\Psi/2)$ where Ψ is the angle included by the bowing arms of the dislocation when it bypasses the precipitate ("the breaking angle"). The critical resolved shear stress is operationally defined by the weakest point in the strongest line that the dislocation encounters in the array. If all of the obstacles have strength β, then the dimensionless critical resolved shear stress τ^* is given by

$$\tau^* = 0.9\beta^{3/2} \tag{1}$$

where

$$\tau^* = \tau l_s b/2T \tag{2}$$

and τ is the critical resolved shear stress, l_s is the mean square obstacle spacing, b is the Burgers vector in the matrix and T is the dislocation line tension [6]. Various solutions for the critical resolved shear stress of a random array of obstacles account differently for the statistical randomness of the array, resulting in a range of values that bracket the constant 0.9 in equation (1) [e.g. 10]. The analytic version of the Hanson and Morris solution given in equation (1) is restricted to values of β less than 0.7. The total volume fraction of precipitates, f, is included through l_s in equation (2), which can be expressed as

$$l_s = d(\pi/6f)^{1/2}.$$

For strong shearable obstacles, the maximum effective obstacle strength is the strength at which Orowan looping is preferred over shear:

$$\beta_c = F_{loop}/2T_{loop}. \tag{3}$$

When the strength of the obstacle is due to its ordered structure, the force required to bypass the obstacle is proportional to its cross-sectional diameter. Consequently, F_{loop} is

proportional to a critical diameter d_{loop} for which the forces required to loop or shear the obstacle are identical, and equation (3) may be rewritten

$$\beta_c = cd_{loop}/2T_{loop}. \tag{4a}$$

The strengths of smaller obstacles scale with the ratio of their diameter to the looping diameter:

$$\beta = \beta_c(d/d_{loop})(T_{loop}/T). \tag{4b}$$

The value of β_c is unity if the effects of dislocation self-interactions are ignored. However, it has been shown that the Orowan stress is strongly affected by self-interactions in materials that are elastically isotropic [11] and anisotropic [12]. The interaction between the arms of the dislocation as it bows out around an obstacle pulls them together. The net effect of this distortion of the dislocation shape is that the force required to make the arms antiparallel (the condition for Orowan looping) is lower than it would be if the dislocation bowed in a circular arc. Conversely, if the elliptically bowed arc that defines the actual looping criterion is approximated by the circular arc assumed in most solutions for the critical resolved shear stress, including the Hanson and Morris solution, then looping occurs before the arms of the dislocation are antiparallel. Bacon, et al. [11] suggest that when the ratio of particle diameter to particle spacing is small this effect can be incorporated into solutions that assume that the dislocation bows in a circular arc. The Hanson and Morris solution may be modified [7] by making the definitions:

$$\beta_c = 0.7$$

and

$$T = (Gb^2/4\pi K) \ln (l_s/b) \tag{5}$$

where K is 1-ν for screw dislocations and one (1) for edge dislocations. Physically, the dependence of the line tension on l_s occurs because self-interaction forces play a smaller role when the obstacles are well separated. It is important to note that equation (4b) implies that the measured looping radius is not a constant, but is instead dependent on the dislocation line tension, which is in turn (equation (5)) dependent on the precipitate spacing.

When the precipitates are ordered, matrix dislocations couple into superdislocations that are total dislocations in the precipitate crystal structure. For materials strengthened by $L1_2$ precipitates (e.g. binary aluminum-lithium alloys and nickel-aluminum superalloys), the dislocations are paired. For a simple pileup of two uncoupled dislocations, the stress on the lead dislocation is twice the applied stress, but in ordered alloys, the stress is further increased by the antiphase boundary area between the coupled dislocations [8]. However, since the critical resolved shear stress in the Hanson and Morris solution is fixed by the strongest line in the array, the configuration in which the applied stress is least magnified (i.e. by a factor of two) determines the critical resolved shear stress (see ref. [7]). Equation (2) should be modified accordingly by multiplying the right side of the equation by two.

The problem of determining the strength of a random array of point obstacles has been addressed both theoretically [6] and by computer simulation [13]. Under the assumptions mentioned above, Hanson and Morris [6] show that for an array of obstacles of different strengths

$$(\tau^*)^2 = \Sigma_i \, x_i(\tau_i^*)^2 \tag{6}$$

where, in analogy to equation (2),

$$\tau_i^* = \tau_i l_s b/2T, \tag{7}$$

where the τ_i are the critical resolved shear stresses for identical arrays composed only of obstacles of type i, the x_i are the volume fractions of these obstacles, and τ is the critical resolved shear stress of the actual array.

It should be noted that the critical resolved shear stress, τ, calculated here represents only the obstacle-controlled portion of the strength of the material and should properly be denoted $\Delta\tau$. Other contributions to the total strength come from the frictional stress provided by the matrix and the grain size.

3. Aging behavior of materials strengthened by a distribution of precipitates

A model that considers the effect of a precipitate size distribution on aging behavior must generate an obstacle distribution that corresponds to a given precipitate size distribution and specify how that distribution evolves with time.

The obstacle distribution can be easily generated for a distribution of spherical precipitates. (The problem is more difficult for plate-like precipitates.) The precipitates may be cut at any cross-section; consequently, each spherical precipitate contributes a series of obstacles with dimensionless diameters $d^* = d/b$

$$d^*_\alpha = [(d^*)^2 - \alpha^2)]^{1/2}$$

where α runs from 0 to $d^*/2$. The obstacle size distribution generated if all the precipitates are the same size (i.e. when the precipitate size distribution can be described as a δ-function) is shown in Figure 1. For a more general precipitate size distribution, the obstacle size distribution is the sum of those for each precipitate size. The obstacles are present in fractions that correspond to the fraction of precipitates in each size range. An obstacle size distribution for a Gaussian precipitate size distribution is shown in Figure 2. Since the maximum effective obstacle diameter is d^*_{loop}, all obstacles with diameters larger than d^*_{loop} are included in the large spike at d^*_{loop}.

The assumptions derived above make it possible to calculate the critical resolved shear stress for a given obstacle distribution using equations (1) - (7). However, as discussed in Section 2, the values of l_s and T that are used in equation (2) to

redimensionalize τ^* will change during aging, so the variation of τ^* is qualitatively different from the variation of τ. Therefore it is convenient to define a second dimensionless strength τ^{**} based on the initial values of the constants that is proportional to the critical resolved shear stress throughout aging

$$\tau^{**} = \tau l_{s,0} b/2T_0. \tag{8}$$

The strengthening contribution of precipitates of type i is then given by

$$\tau_i^{**} = 0.9(\beta_i)^{3/2}(l_s/l_{s,0})(T_0/T) \tag{9}$$

where β_i is the strength of an obstacle of type i, defined in equation (4), and l_s and T are defined for the entire array at the same time as τ_i^{**}. Equation (9) may be rewritten so that it depends only on the obstacle strengths and the initial constants $l_{s,0}$ and T_0. The full equation which is quadratically summed using equation (6) and the fraction of precipitates with each diameter d_i and then redimensionalized using equation (8) is

$$\tau_i^{**} = 0.9(l_s/l_{s,0})(T_0/T)(2/d_i^*)^{1/2}(T_{loop}/T)^{3/2}(\beta_c)^{3/2}\Sigma_\alpha (d_{i\alpha}^*/d_{loop}^*)^{3/2} \tag{10}$$

where the index α runs from 0 to $d^*/2$ and $d_{i\alpha}^*$ cannot exceed d_{loop}^*, the maximum effective obstacle diameter. The additional terms in equation (10) are from the expansion of β_i. The factor of $(2/d_i^*)^{1/2}$ is included so that the number of obstacles contributed by the sum is unity (the fraction is fixed by x_i in the quadratic sum). The values of $l_{s,0}$ and l_s for a precipitate size distribution may be determined analogously to the single precipitate size case. The dependence on volume fraction appears through the dependence on l_s.

Predicting the shape of the aging curve requires generating the precipitate size distribution as a function of time from a single measured (or defined) precipitate size distribution. The discussion of aging behavior below makes three assumptions about the evolution of the precipitate size distribution: 1) that the precipitate size distribution coarsens self-similarly with respect to the ratios $d/\langle d\rangle$; 2) that the total volume fraction of precipitates is constant in the region of the aging curve under study; and 3) that coarsening obeys the Lifshitz-Slyozov-Wagner (LSW) rule,

$$d^3 - d_0^3 = kt$$

where d_0 is a constant and k is the LSW constant, so that the variation in strength with precipitate size can be related to strength as a function of aging time. The coarsening rule may be restated in dimensionless form in terms of a dimensionless time $t^* = kt/d_0^3$ as

$$d^*/d_0^* = (t^*)^{1/3}$$

for $t^* \gg 1$. The validity of these assumptions for binary aluminum-lithium alloys will be considered in the next section. The assumption of constant volume fraction is easily dropped by varying l_s at each point along the aging curve, but is included for simplicity.

A quantitative comparison illustrating the magnitude of the effect of precipitate size distribution width on aging behavior for three Gaussian distributions is shown in figure 3. Peak strength for the δ-function distribution is approximately ten percent higher than for the wide Gaussian distribution, but it occurs later. These results may be qualitatively explained by considering the functional dependence of strength (equation (10)) on precipitate size and aging time. If all of the obstacles have the same strength, these relationships are greatly simplified. Before the looping diameter is reached the critical resolved shear stress is proportional to $d^{1/2}$ or $t^{1/6}$; when the precipitates are greater than the looping diameter in size, the critical resolved shear stress is proportional to d^{-1} or $t^{-1/3}$ (the effective strength remains constant, but l_s continues to increase). The obstacle size distribution weakens these dependences and eliminates the sharp cusp in the dependence of the critical resolved shear stress on obstacle diameter that occurs at the looping diameter. However, it is still true that the critical resolved shear stress depends more strongly on precipitate size after looping than before. Consequently, if a distribution of precipitate sizes exists, peak strength will occur almost immediately after the largest of the precipitates reaches the looping diameter, not when the average-sized precipitate reaches the looping diameter. By contrast the amount of strengthening provided by the precipitates is most closely related to the average precipitate diameter. As a result, the maximum achievable strength increases as the distribution narrows. As illustrated schematically in figure 4, when the largest precipitates reach the looping diameter, the average precipitate radius for a narrow distribution is greater than the average radius of a broad distribution of the same volume fraction. The strength of the distribution is correspondingly higher. Thus, the critical resolved shear stress at peak strength is maximized if all the precipitates are the same size.

4. Sample calculation for a binary aluminum-lithium alloy

Binary aluminum-lithium alloys are an excellent model system with which to test the usefulness of the solution to the critical resolved shear stress model described above because these alloys nearly satisfy the idealizations of the model. The physical metallurgy of this system has been extensively studied [14,15]. A comparison of assumptions of the solution with experimental observations of this system precedes the critical resolved shear stress calculations. A more detailed discussion of the experimental data may be found in Glazer [9].

Precipitate: The alloys are hardened by the face-centered cubic based ordered $L1_2$ precipitate δ' [16,17]. This precipitate is the only obstacle that contributes importantly to the strength of the alloy. The precipitates are spherical [18] and are neither observed nor expected to change shape as they coarsen [19,20]. The misfit of these precipitates is extremely small (~ -0.1 %) (see for example, [21,22]), so the strengthening contribution is almost entirely due to the ordered structure of the precipitate and is a function of the sheared cross-sectional diameter only. The looping diameter has been measured and lies between 40 and 60 nm [7]. As discussed in Section 2, the looping radius depends on the mean square obstacle spacing when the sample was deformed (see ref. [7] for a more extensive discussion). The value of 50 nm reported by Furukawa, et al. [23] for a mean square obstacle of 275 nm was selected for the computations described below. The Burgers vector in aluminum is approximately 0.29 nm.

Precipitate coarsening: The precipitates coarsen according to LSW even at very small sizes (e.g. [18,24]). Precipitate size distributions have been measured and found to coarsen in a self-similar fashion [5,25]. The interfacial energy of the precipitates in the aluminum matrix is small (e.g. [26]), so the volume fraction is essentially constant during coarsening for reasonable initial volume fraction and precipitate size [9]. Evidently, the assumptions about the evolution of the precipitate size distribution in Section 3 are satisfied.

Dislocations: As discussed by Glazer and Morris [7], screw dislocations are observed to control deformation in aluminum-lithium alloys. The dislocations are observed to move as superdislocation pairs. The effect of this pairing is that the actual stress at the obstacle is twice the applied stress (see Section 2). In the overaged condition, when Orowan looping is the dominant deformation mechanism, the dislocations are not coupled [22,27]; consequently, the applied stress is no longer multiplied and the strength of the material is comparatively increased. Presumably, at and slightly beyond peak strength, when both shearing and looping are important mechanisms, the dislocations are weakly coupled.

Direct comparison of the theoretically predicted and experimentally measured strengthening increment during the aging process is possible for the precipitate size distribution reproduced in figure 5 from Gu, et al [5] for Al-2.7Li-0.3Mn aged at 200°C. The Mn in this alloy is precipitated in the form of Al-Mn dispersoids and does not affect the aging behavior. Theoretical aging curves were calculated using a looping diameter of 50 nm and a corresponding value of the mean square obstacle spacing of 275 nm. The calculations use a shear modulus of 30 GPa. The experimental and theoretical aging curves are shown in figure 6. The theoretical coarsening rate has been fixed using the experimentally determined rate constant [5]. Since the quenched alloy undoubtedly contains some atom clusters, the theoretical aging curve has been shifted to slightly shorter aging times to obtain the best fit. The strength increment for both yield strength curves is the increase over the lowest measured strength. To convert theoretical critical resolved shear stress values to yield strengths a Taylor factor of 3 has been assumed. Figure 6 shows that the theoretical and experimental aging curves are in excellent agreement up to peak strength. Beyond peak strength the model is no longer valid since it does not account for the uncoupling of paired dislocations after Orowan looping begins. As described above, this uncoupling would cause the strength to drop off more gradually after the peak than it would if the dislocations remained coupled. The difference between the experimental and theoretical curves in the figure in this regime is therefore as expected.

It should be noted that this plot differs slightly from the one in references 19 and 28 both in the choice of looping diameter and in the proper incorporation of the fact that much of the lithium remains in solution. Many more experimental measurements of the looping diameter are now available, and a looping diameter of 50 nm rather than 60 nm now seems appropriate.

5. Discussion

Previous studies of aging behavior

Melander and coworkers have previously calculated aging behavior using measured precipitate size distributions for various alloys including some hardened by ordered precipitates using a slightly improved version of the Hanson and Morris solution [2]. The solution described here is similar; it differs from Melander and Persson's work chiefly in the handling of the dislocation line tension and the related topic of dislocation self-interactions. Melander and Persson use the deWit-Koehler form of the line tension given by Ardell [8], but with an adjustable parameter to describe the amount of edge or screw character of the dislocation. This fitting parameter is varied along the aging curve as the strength of the precipitates increases. The fitting parameter, the value of β_c, and the measure of length in the logarithmic term (here l_s/b) are found iteratively from the average precipitate strength and segment length along the strong line. This iterative approach seems unnecessarily cumbersome since the fundamental shortcoming of the Hanson and Morris solution for this application, the assumption that the dislocation bows in a circular arc and does not interact with itself, is still not addressed. The approach used here is simpler and eliminates the fitting parameter from formulation of the line tension.

Advantage of uniform precipitate size distribution.

As discussed previously, the model of order hardening described here predicts that for a fixed volume fraction a narrow precipitate size distribution will age to a higher peak strength than a broad precipitate size distribution. The critical resolved shear stress is maximized if the distribution is a δ-function. The effect of the width of the precipitate size distribution with an average diameter <d> on the critical resolved shear stress (as opposed to the maximum strength achievable by coarsening a precipitate size distribution) has been investigated previously by computer simulation [29,30], theoretical analysis [7,19,30] and experimental studies [4]. The formalism of this study permits the apparently different results of these authors to be reconciled.

Foreman and Makin [29] considered the effect of distribution width for two types of obstacle distributions in their computer simulations: square breaking angle spectra (biased toward strong obstacles) and square obstacle strength spectra. Their results indicate that widening the distribution symmetrically strengthens the array (because stronger obstacles are included). When the distribution is widened by adding weak obstacles, the critical resolved shear stress for a given volume fraction of obstacles decreases. Altintas [30] considered the same cases analytically using the Hanson and Morris strong line solution [6] and was able to closely reproduce the computer simulation results.

Munjal and Ardell [4] attempted to measure experimentally the effect of the width of the precipitate size distribution on the critical resolved shear stress in a Ni-Al alloy aged to near peak strength. They found that a 30% increase in the width of the precipitate size distribution corrected to constant volume fraction resulted in an 8% decrease in the

strengthening increment near peak strength due to precipitation. Because this difference is much larger than that predicted by Foreman and Makin for the same case, Munjal and Ardell suggest that the finite size of the obstacles may play an important role. However, there are two reasons for believing that these results can be viewed as consistent with point obstacle models: firstly, as they realized, the method of comparison selected by Munjal and Ardell is biased toward strong obstacles, and secondly, the comparison between precipitate size distributions is made at fixed average precipitate radius without regard for the size of the precipitates relative to the looping diameter. To begin with, Munjal and Ardell compare a breaking angle histogram computed from the measured distribution of precipitate radii (rather than from the corresponding distribution of obstacles) with the square breaking angle distribution of the same standard deviation studied by Foreman and Makin. The histograms generated by Munjal and Ardell are both narrower and more biased toward strong obstacles than the actual obstacle strength histogram. Both of these errors lessen the size of the distribution width effect predicted by Foreman and Makin, so their results are not necessarily inconsistent. Secondly, the critical resolved shear stresses are compared at a fixed average precipitate diameter that corresponds to peak strength for the narrower precipitate size distribution. Since widening the distribution causes peak strength to occur at a smaller average precipitate diameter, the distribution is overaged at this point. Consequently, the observed decrease in strength is greater than the difference between the peak strengths associated with the distributions. If Munjal and Ardell had chosen to fix the average radius at the peak strength of the wider distribution, they might have concluded that widening the distribution increased the critical resolved shear stress.

Obstacle strength summing rules

The applicability of the quadratic sum to the problem of summing the contributions of obstacles of varying strength to the critical resolved shear stress was asserted earlier on theoretical grounds, despite the debate in the literature [8,9]. However, there is considerable justification for the use of the quadratic sum, the basis of which is outlined below. All of the formulae take the form

$$(\tau^*)^q = \sum_i (x_i)^{q/2} (\tau_i^*)^q.$$

There are only three values of q that have been theoretically justified for obstacle strengthening: two (2) (the quadratic sum given in equation (1)) for distinct point obstacles by Hanson and Morris [6], three-halves (3/2) which was predicted by Labusch [31] for diffuse obstacles, and one (1) for *regular* arrays of obstacles [32]. More recently, a number of researchers have found it necessarily to invoke other, variable, values of q to fit their experimental data with theory [33-35]. While summing theories with values of q less than 2 may be valid in certain regimes, it is disturbing that for a combination of weak and strong obstacles

$$\lim_{x_s \to 0} \quad d\tau/dx_s \to \infty \quad q < 2$$

$$\to 0 \quad q \geq 2$$

where x_s is the fraction of strong obstacles [8,30].

The Hanson and Morris derivation of the quadratic sum restricts the dimensionless obstacle strength ß to values less than 0.7. Good agreement with the quadratic sum is not expected for larger values of ß. The key question is whether obstacles with high strengths (ß » 0.7) actually occur. As mentioned earlier, dislocation self-interactions limit the effective value of ß in a circular bow-out model to ~0.7 [7]. Furthermore, Foreman and Makin's simulations [29], which also assume that the dislocation bows in a circular arc, indicate that when obstacles described by very large values of ß dominate the array, long fingers of the dislocation move forward along paths of easy movement, eventually encircling groups of obstacles. This type of motion seems unphysical and does not provide a suitable test of summing rules, yet the two cases considered by Foreman and Makin that are often cited as evidence against the quadratic sum rule include obstacles of this sort (ß > 0.9). For values of ß less than 0.7, the quadratic sum rule seems adequate to describe the existing computer simulation data [29,30]. Altintas examined a number of cases by computer simulation using obstacles with strength ß < 0.1 [30]. In all of the cases he considered, the quadratic sum is an adequate description of the observed behavior; unfortunately, in this strength regime the difference between a quadratic sum and a linear one (q=1) is not that great, even when the obstacles have widely differing strengths. Efforts to study summing behavior in actual systems are hampered by questions about other aspects of the relevant strengthening theory that cast doubt on the accuracy of predictions of the strength of the individual obstacles [34,36].

Finally, the dimensionless form of the quadratic sum rule given in equation (6) is often quoted in the literature [8,37] as providing a theoretical justification for the summing rule

$$(\tau)^2 = \sum_i x_i(\tau_i)^2 \qquad (11)$$

first proposed by Koppenaal and Kuhlman-Wilsdorf [38]. The empirical justification for equation (11) is that it relates the critical resolved shear stress to the average free segment length along the dislocation line. However, it should be noted the quadratic sum rule for the dimensionless critical resolved shear stress only implies equation (11) if the dimensionalizing factors for the critical resolved shear stress – l_s, b and T – are constant for all the τ_i. There is no theoretical basis for equation (11) without these restrictions. In many of the efforts to verify this summing rule experimentally by isolating obstacle types [for example, 33,35], this requirement is not met. The values of l_s and T must be determined for each experimental case and used to compute values of τ_i^* which can then be compared with the predictions of the dimensionless quadratic sum rule given in equation (6). A different calculation for the summing exponent q will lead to a different (non-quadratic) dependence of the strength on the value of q. However, these values of q cannot be generalized beyond the specific cases for which they experimentally determined.

6. Conclusion

The aging behavior of a material strengthened by ordered precipitates is sensitive to the precipitate size distribution primarily near peak strength. The onset of peak strength occurs when the size of largest precipitates in the distribution reaches the looping diameter. The value of peak strength is principally determined by the average precipitate diameter at that point. Thus, the strength is maximized if all of the precipitates are the same size. This qualitative approach was used to reconcile apparently conflicting results of previous authors regarding the effect of precipitate size distributions on the critical resolved shear stress. The quantitative accuracy of the model comes from the use of the Hanson and Morris strong line solution as modified to account for dislocation self-interactions. This modified solution sets the maximum value of the dimensionless obstacle strength ß at 0.7. In this strength regime, the quadratic sum rule seems to describe obstacle strength summing behavior adequately. The assumptions of the model are relatively accurate for binary aluminum-lithium alloys. There is good agreement between the predictions of the model and experimental data on a binary aluminum-lithium alloy.

Acknowledgment

The authors would like to thank Prof. A.J. Ardell for helpful discussions of this work. This study was jointly supported by the Aluminum Company of America and the Director, Office of Energy Research, Office of Basic Energy Science, Material Sciences Division of the U.S. Department of Energy under Contract No. DE-AC03-76SF00098. J. Glazer is supported by an AT&T Bell Laboratories PhD Scholarship.

References

1. A. Melander and P.Å. Persson, *Acta Metall.*, **26**, 267 (1978).
2. A. Melander and P.Å. Persson, *Met. Sci.*, **13**, 391 (1978).
3. A. Melander and P.Å. Persson, *Scand. J. Metall.*, **7**, 181 (1978).
4. V. Munjal and A.J. Ardell, *Acta Metall.*, **24**, 827 (1976).
5. B.P Gu, G.L. Liedl, J.H. Kulwicki and T.H. Sanders, Jr., *Mat. Sci. Eng.*, **76**, 217 (1985).
6. K. Hanson and J.W. Morris, Jr., *J. Appl. Phys.*, **46**, 983 and 2378 (1975).
7. J. Glazer and J.W. Morris, Jr., *Phil. Mag. A*, submitted. LBL Report no. 22738 (1986).
8. A.J. Ardell, *Met. Trans. A*, **16**, 2131 (1985).
9. J. Glazer, M.S. Thesis, University of California, Berkeley, CA (1986).
10. R. Labusch, *J. Appl. Phys.*, **48**, 4550 (1977).
11. D.J. Bacon, U.F. Kocks and R.O. Scattergood, *Phil. Mag.*, **28**, 1241 (1973).
12. R.O. Scattergood and D.J. Bacon, *Phil. Mag.*, **31**, 179 (1975).
13. S. Altintas and J.W. Morris, Jr., *Acta Metall.*, **34**, 801 and 809 (1986).
14. "Proceedings of the 2nd International Conference on Aluminum-Lithium Alloys," T.H. Sanders, Jr. and E.A. Starke, Jr., eds., AIME, Warrendale, PA (1983).
15. "Proceedings of the 3rd International Conference on Aluminum-Lithium Alloys," C. Baker, et al., eds., The Institute of Metals, London (1986).

16. J.M. Silcock, *J. Inst. Met.*, **88**, 357 (1960).
17. B. Noble and G.E. Thompson, *Met. Sci.*, **5**, 114 (1971).
18. J.H. Kulwicki and T.H. Sanders, Jr., in "Proceedings of the 2nd International Conference on Aluminum-Lithium Alloys," T.H. Sanders, Jr. and E.A. Starke, Jr., eds., AIME, Warrendale, PA, p. 31 (1986).
19. J. Glazer, T.S. Edgecumbe and J.W. Morris, Jr., in "Proceedings of the 3rd International Conference on Aluminum-Lithium Alloys," C. Baker, et al., eds., The Institute of Metals, London, p. 369 (1986).
20. W. Muller, E. Bubeck and V. Gerold, *ibid* , p.435.
21. S.F. Baumann and D.B. Williams, in "Proceedings of the 2nd International Conference on Aluminum-Lithium Alloys," T.H. Sanders, Jr. and E.A. Starke, Jr., eds., AIME, Warrendale, PA, p. 17 (1986).
22. P. Sainfort and P. Guyot, in "Proceedings of the 3rd International Conference on Aluminum-Lithium Alloys," C. Baker, et al., eds., The Institute of Metals, London, p. 420 (1986).
23. M. Furukawa, Y. Miura and M. Nemoto, *Trans. JIM,* **26**, 230 (1985).
24. S.F. Baumann and D.B. Williams, *Met. Trans.*, **16A**, 1203 (1985).
25. B.P. Gu, G.L. Liedl, K. Mahalingham and T.H. Sanders, Jr., *Mat. Sci. Eng.*, **77**, 71 (1986).
26. S.F. Baumann and D.B. Williams, *Scr. Met.*, **18**, 611 (1984).
27. Y. Miura, A. Matsui, M. Furukawa and M. Nemoto, in "Proceedings of the 3rd International Conference on Aluminum-Lithium Alloys," C. Baker, et al., eds., The Institute of Metals, London, p. 427 (1986).
28. J. Glazer and J.W. Morris, Jr., in "Aluminum Alloys: Their Physical and Mechanical Properties," E.A. Starke, Jr., ed., Engineering Materials Advisory Service, Ltd. (1986).
29. A.J.E. Foreman and M.J. Makin, *Can. J. Phys.*, **45**, 511 (1967).
30. S. Altintas, PhD thesis, University of California, Berkeley, CA (1978).
31. R. Labusch, *Phys. Stat. Sol.*, **41**, 659 (1970).
32. U.F. Kocks, A.S. Argon and M.F. Ashby, *Prog. Mat. Sci.*, **19**, 1 (1975).
33. J. Huang and A.J. Ardell, "Aluminum Technology '86," Book 3, Session 3, conference preprint, London, March 11-13, 1986, Institute of Metals (1986).
34. N. Buttner and E. Nembach, in "Deformation of Multi-Phase and Particle Containing Materials," Proceedings of the 4th Risø International Syposium on Metallurgy and Materials Science, J.B. Bilde-Sorensen, et al., eds., Risø National Laboratory, Roskilde, Denmark, p. 189 (1983).
35. E. Nembach and G. Neite, *Prog. Mat. Sci.*, **29**, 177 (1985).
36. E. Nembach and M. Martin, *Acta Metall.*, **28**, 1069 (1980).
37. U.F. Kocks, *Mat. Sci. Eng.*, **27**, 291 (1977).
38. T.J. Koppenaal and D. Kuhlman-Wilsdorf, *Appl. Phys. Lett.*, **4**, 59 (1964).

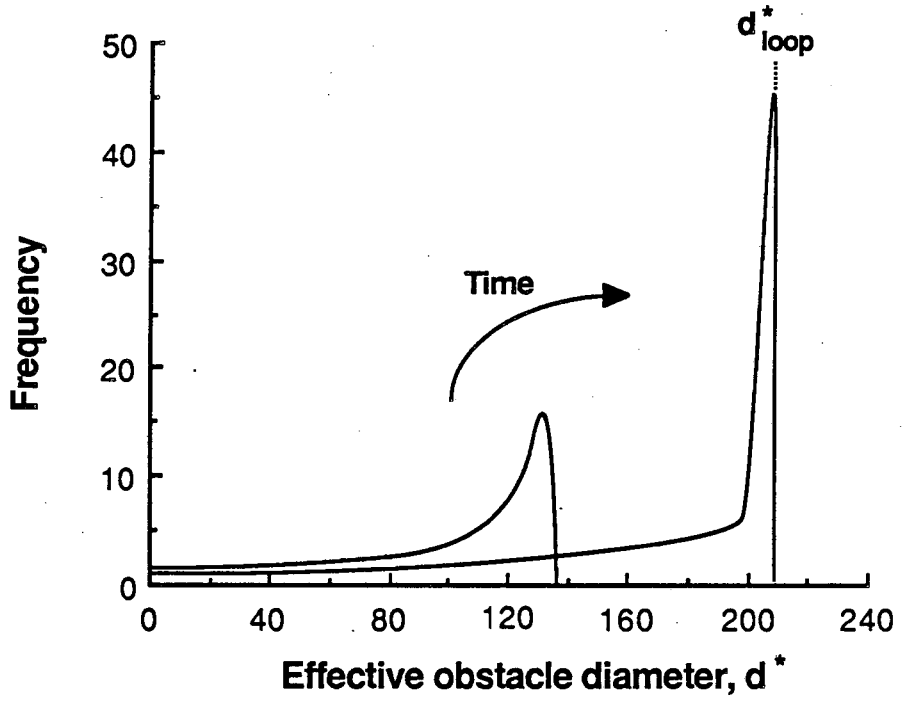

Figure 1 Distribution of effective obstacle diameters for precipitates of uniform size. The dimensionless looping radius is $d^*_{loop} = 210$.

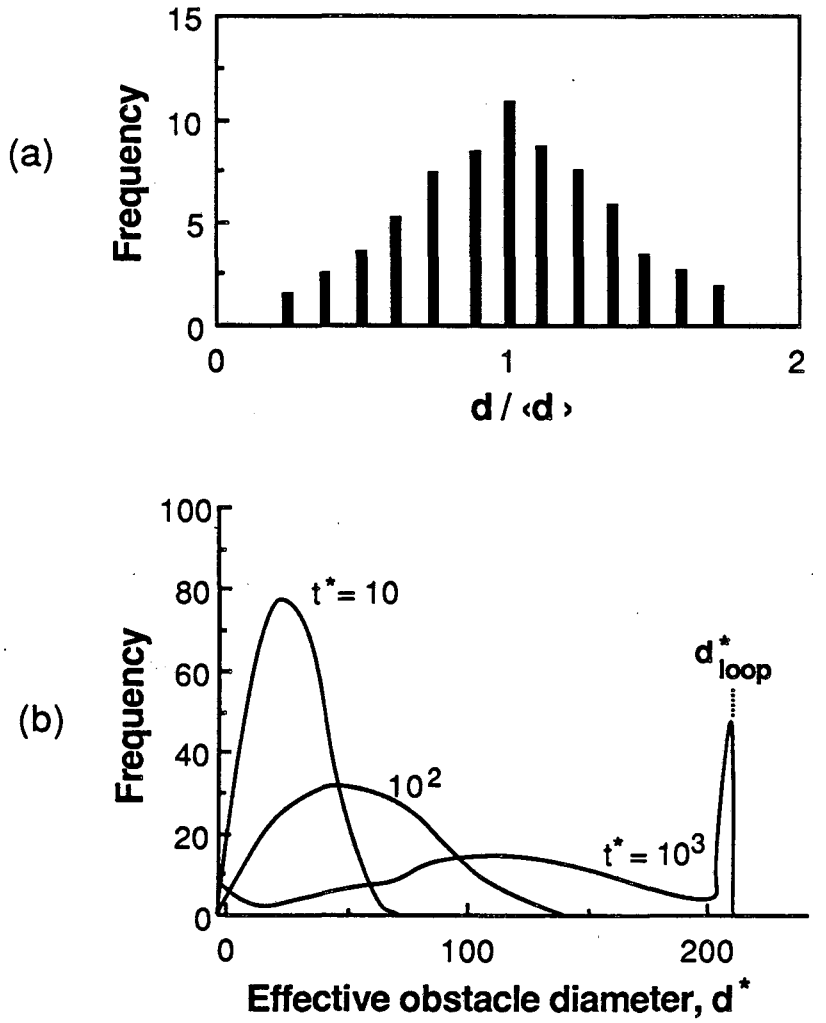

Figure 2 Effective obstacle diameter distribution for a Gaussian precipitate size distribution coarsening at fixed volume fraction. (a) Precipitate size distribution at dimensionless time t*= 0. (b) Obstacle distribution at various times for dimensionless looping radius $d^*_{loop} = 210$.

(a)

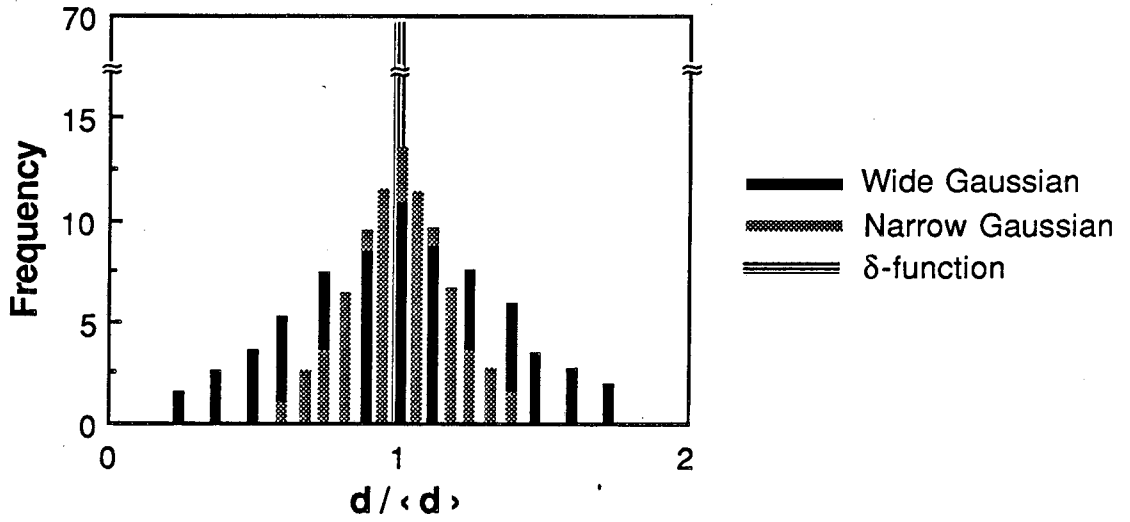

(b)

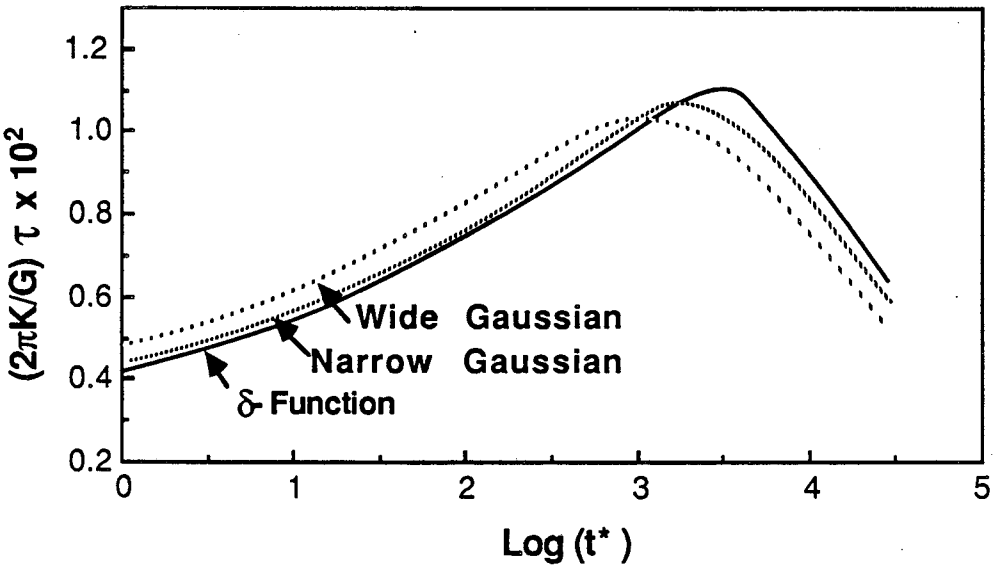

Figure 3 Comparison of calculated aging curves for three precipitate size distributions of different width. (a) Histograms of the precipitate size distributions corrected to constant volume fraction. (b) Aging curves calculated for $\langle d^* \rangle = 16$ at $t^* = 0$, $f = 0.2$ and $d^*_{loop} = 210$. The dislocations are assumed to be uncoupled.

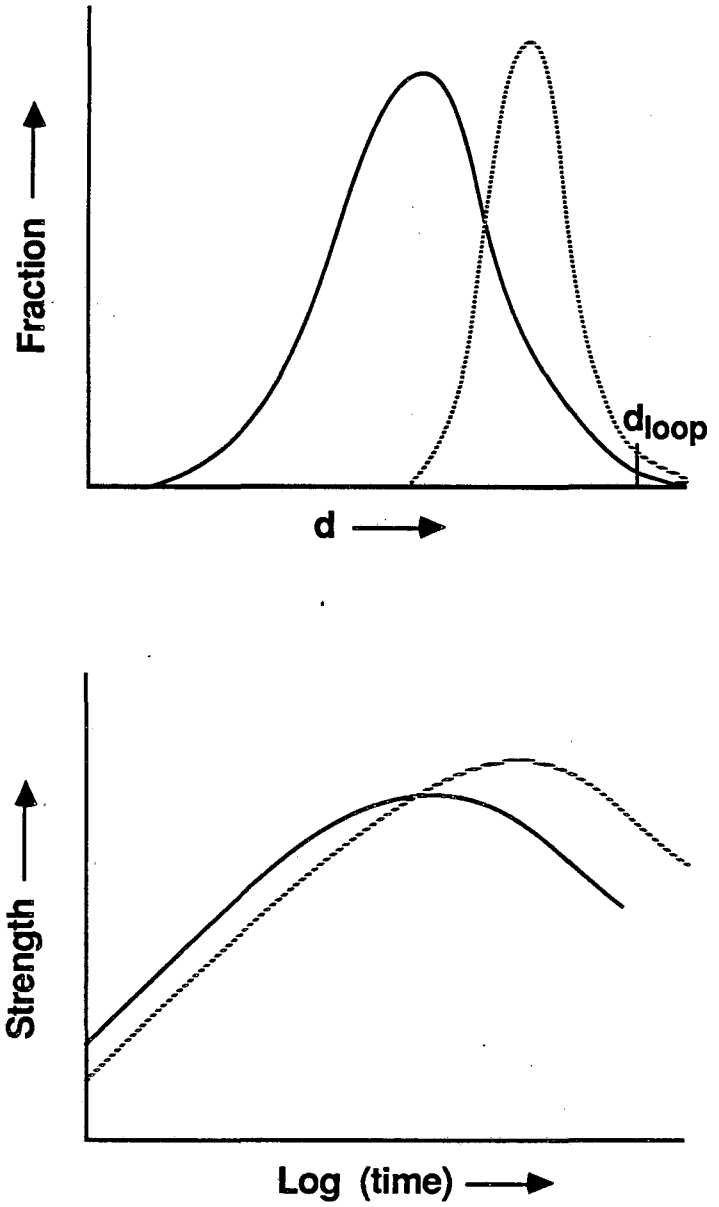

Figure 4 Schematic comparison of the aging behavior of a narrow and a wide precipitate size distribution. The peak strength of the narrow distribution is greater and occurs later. The effect of the distribution width is exaggerated for clarity.

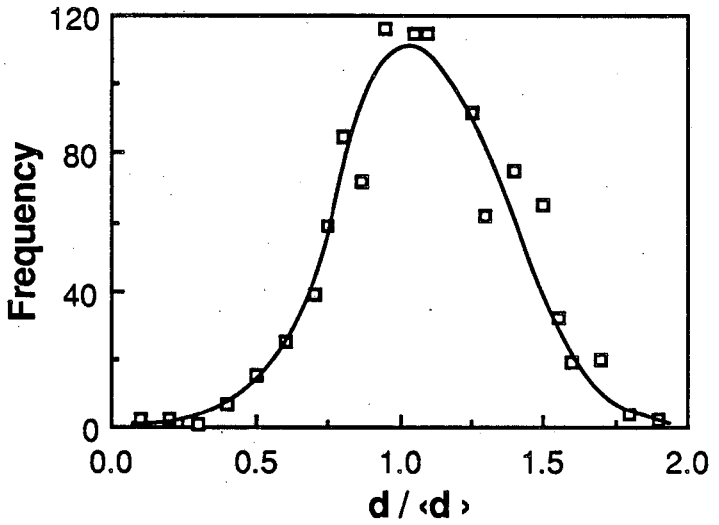

Figure 5 Precipitate size distribution measured by Gu, et al [5] for an Al-2.8Li-0.3Mn alloy aged 48 hours at 200°C.

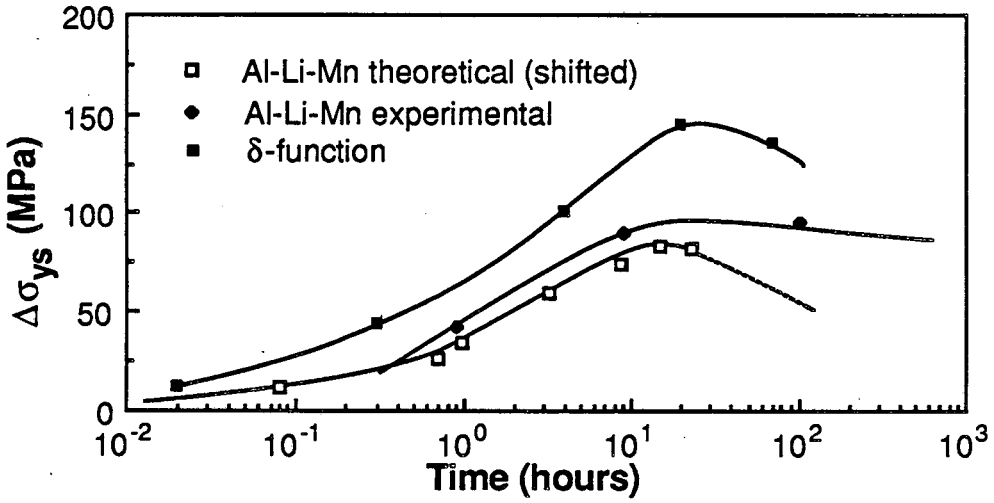

Figure 6 Comparison of experimentally measured and predicted aging curves for the precipitate size distribution of Figure 5. The experimental curve is taken from ref. 5. The theoretical curve is shifted to slightly shorter aging times to account for atom clustering. The predicted aging curve for a δ-function precipitate size distribution with the same average precipitate diameter and volume fraction is shown for comparison.

LAWRENCE BERKELEY LABORATORY
TECHNICAL INFORMATION DEPARTMENT
UNIVERSITY OF CALIFORNIA
BERKELEY, CALIFORNIA 94720